JOURNAL OF PHYSICAL ORGANIC CHEMISTRY
J. Phys. Org. Chem. 2007; **20:** 677–684
Published online 27 July 2007 in Wiley InterScience
(www.interscience.wiley.com) DOI: 10.1002/poc.1230

Kinetics and thermodynamics of the Li/Li^+ couple in tetrahydrofuran at low temperatures (195–295 K)

Christopher A. Paddon,[1] Sarah E. Ward Jones,[1] Farrah L. Bhatti,[2] Timothy J. Donohoe[2] and Richard G. Compton[1]*

[1]Physical and Theoretical Chemistry Laboratory, University of Oxford, South Parks Road, Oxford OX1 3QZ, UK
[2]Chemistry Research Laboratory, University of Oxford, Mansfield Road, Oxford OX1 3TA, UK

Received 22 February 2007; revised 20 April 2007; accepted 15 May 2007

ABSTRACT: Kinetic and thermodynamic (formal potential) data relating to the synthetically useful Li/Li^+ couple in tetrahydrofuran (THF) solvent at a range of temperatures (196–295 K) are reported. Formal potentials, E_f^0 have been measured *versus* the standard reference electrode, $Fc(4\,mM)/Fc^+PF_6^-(4\,mM)$) in THF. At 295 K the following data have been obtained using a mathematical model to simulate the electro-deposition (metal deposition and growth kinetics) processes of lithium (Li) on a platinum microelectrode; a E_f^0 of -3.48 ± 0.005 V, $dE_f^0/dT = -9.2\ (\pm 0.5) \times 10^{-4}\,V\,K^{-1}$, the standard electrochemical rate constant, $k_0 = 1\ (\pm\ 0.1) \times 10^{-4}\,cm\,s^{-1}$, transfer coefficient, $\alpha = 0.57 \pm 0.03$ and diffusion coefficient, $D = 8.7 \pm 0.1 \times 10^{-6}\,cm^2\,s^{-1}$. Copyright © 2007 John Wiley & Sons, Ltd.

KEYWORDS: Li/Li^+ redox couple; tetrahydrofuran; formal potential; metal nucleation and growth kinetics; electro deposition; electrochemical rate constant

INTRODUCTION

Lithium (Li) as a reducing agent in organic synthesis is well known,[1] and its applications diverse. For example, Li metal has been used in the reductive opening of heterocycles,[2] reaction with benzil[3] and vinylsilanes,[4] reductive coupling of carbonyl compounds[5,6] and in the synthesis and reduction of certain spiro-compounds.[7] Recent interest into alkali-metal/arene-based reductions in aprotic media are also becoming popular.[1,2,8–16] Further, many cyclic voltammetry (CV) studies in aprotic solvents have shown the tendency of organic radical anions, and dianions, to undergo ion-pairing phenomena[17–19] and significant differences in the shifting of radical anion reduction peaks have been observed in the CV responses of quinones upon changing the cation of the supporting electrolyte, namely R_4N^+ (R = alkyl) or Li^+.[20–24] Li ion-pairing effects on the electrochemical behaviour of quinonemethides,[25,26] which constitute key intermediates in natural lignan biosynthesis (electrochemical biomimetic syntheses), have been reported.[27] More recently, the Li^+ cation was highlighted has having an 'overriding importance' for the 'orientation' of the oxidative coupling of 4-hydroxycinnamate derivatives by intercalation.[28]

From a technological view-point, the development of Li ion batteries and industrial reactors[29] with good performance, safety, stability and reliability has also been an active area of research for the past 3 decades.[30–35] Many of the Li ion batteries employ an aprotic medium containing a Li salt stemming from the early work by Koch and co-workers.[36–45] However, there is often uncertainty as to the stability of the media to Li metal, the kinetics and thermodynamics of the Li/Li^+ couple, the role of water and other impurities in the electrolyte and the identity and role of surface films on the Li metal.[46–51] Although many attempts have been made to use modern electrochemical techniques to gain a more fundamental knowledge of the Li/Li^+ couple, the data are often distorted particularly in resistive solvents,[52] and hence, our present knowledge of the Li/Li^+ couple is rather less than its practical applications.

In this paper we describe and present simulations of the electro deposition of bulk Li on a platinum microdisc-surface from a solution containing Li^+ salts enabling both kinetic and thermodynamic (formal potential, E_f^0) for the Li/Li^+ couple in tetrahydrofuran (THF) to be determined. In addition, the Li/Li^+ couple has been investigated over a range of temperatures: 295–196 K.[53–56] In particular, E_f^0 was measured *versus* the standard reference electrode, $Fc/Fc^+PF_6^-$ in THF. Previous work has been published by Fawcett co-workers,[57] Wiesener *et al.*[58] and Pletcher and co-workers[59–62] who used copper microelectrodes and based electrochemical measurements

**Correspondence to:* R. G. Compton, Physical and Theoretical Chemistry Laboratory, University of Oxford, South Parks Road, Oxford OX1 3QZ, UK.
E-mail: richard.compton@chem.ox.ac.uk

against the Li/Li^+ couple only, and in ethereal solvents. So far, however, no simulations or model has been presented to describe the electro-deposition mechanism displayed by Li/Li^+ in aprotic solvents. The thermodynamic reduction potential, E_f^0 of Li can be compared to that of various organic compounds in a common solvent system allowing a preliminary assessment of the reduction capabilities of the metal. Owing to the huge number of applications of the Li/Li^+ couple, from modern energy advances to biomimetic syntheses, further insight into the kinetics and thermodynamics is of importance and the purpose underpinning this paper.

EXPERIMENTAL

Reagents

Lithium hexafluoroarsenate ($LiAsF_6$) (V) (98%), (Aldrich); tetra-*n*-butylammonium perchlorate, (Fluka), were used as received without any further purification. Anhydrous THF was purified by filtration through two columns of activated alumina (grade DD-2) as supplied by Alcoa, employing the method of Grubbs co-workers.[63]

Cyclic voltammetry (CV)

Voltammetric measurements were carried out on an Autolab PGSTAT 20 (Eco-Chemie, Utrecht, Netherlands) potentiostat. A three-electrode arrangement was used in an airtight, three-necked electrochemical cell. The cell with solid electrolyte was dried *in vacuo* overnight before solvent addition and electrochemical experiments. The working electrodes used were a platinum microdisc electrode (ESA Biosciences, US, radius: 5.0 μm), a platinum macrodisc electrode housed in Teflon™ (area, $A = 0.0104\,cm^2$) and a large area, shiny platinum wire (Goodfellow Cambridge Ltd, Cambridge, UK) was employed as the counter electrode. The working electrodes were carefully polished before use on a clean polishing pad (Kemet, UK) using 3 and 1 μm diamond spray (Kemet, UK). Each working electrode was then rinsed in de-ionised and doubly filtered water of resistivity no greater than 18 MΩ cm, taken from an Elgastat filter system (Vivendi, Bucks, UK) and carefully dried prior to use. A $Fc/Fc^+PF_6^-$ (both in equimolar concentration; 4 mM) reference electrode was developed for use in THF and at low temperatures and has been described previously.[64] The temperature was monitored and controlled by an external system (Julabo FT902, JULABO Labortechnik GmbH, D-77960 Seelbach/Germany) accurately (±1 K). Typically the solutions were degassed vigorously for 5 min using impurity-free argon (BOC gases, Guildford, Surrey, UK) to remove any trace oxygen and an inert atmosphere was maintained throughout all analyses. All solutions were prepared under an atmosphere of argon using oven-dried glassware such as syringes and needles used for the transfer of moisture sensitive reagents. All voltammetric measurements were performed inside a Faraday cage in order to minimise any background noise.

THEORY

Mathematical model

We consider the deposition and stripping of Li under CV conditions from a microdisc electrode of radius, r_d. It is assumed that the rate of dissolution of Li from the surface is independent of the amount present on the surface whereas the rate of deposition is dependent on the solution concentration. The electrode reaction of interest is assumed to follow a one-electron transfer mechanism and display Butler–Volmer kinetics:[65,66]

$$Li^+(sol) + e^- \underset{k_b}{\overset{k_f}{\rightleftharpoons}} Li(s) \tag{1}$$

where the Li^+ ions are in solution and Li is a solid on the electrode surface. The local position dependent coverage of Li on the microdisc, Γ_{Li}, is initially zero across the whole disc. The height of any deposit formed will be ignored and as such the microdisc will always be approximately modelled as a flat disc.[67] k_f and k_b are the forward and backward rate constants defined by:

$$k_f = k_0 \exp\left(\frac{-\alpha F}{RT}(E - E_f^0)\right), \tag{2}$$

$$k_b = k_0[Li^+]^0 \exp\left(\frac{(1-\alpha)F}{RT}(E - E_f^0)\right) \tag{3}$$

where k_0 is the surface process rate constant for the Li^+/Li couple with units of $cm\,s^{-1}$, α is the transfer coefficient and E_f^0 is the formal potential. $[Li^+]^0$ is the standard concentration equal to $1 \times 10^{-3}\,mol\,cm^{-3}$ and is included to reflect the different standard states of Li and Li^+. R is the ideal gas constant ($8.314\,J\,K^{-1}\,mol^{-1}$), F is Faraday's constant ($96\,485\,C\,mol^{-1}$) and T is the absolute temperature in K.

The mass transport in solution of Li^+ to and from the electrode surface is given by the following partial differential equation (Fick's first law):[66]

$$\frac{\partial[Li^+]}{\partial t} = D\left(\frac{\partial^2[Li^+]}{\partial r^2} + \frac{1}{r}\frac{\partial[Li^+]}{\partial r} + \frac{\partial^2[Li^+]}{\partial z^2}\right) \tag{4}$$

using the cylindrical coordinate system shown in Fig. 1 and where D is the diffusion coefficient of Li^+. Due to the cylindrical symmetry only the plane highlighted needs to be simulated. The change in the local position dependent surface coverage, Γ_{Li}, with time is described by the following equation:

$$\frac{\partial\Gamma_{Li}}{\partial t} = k_f[Li^+]_{surf} - k_b \tag{5}$$

DOI: 10.1002/poc

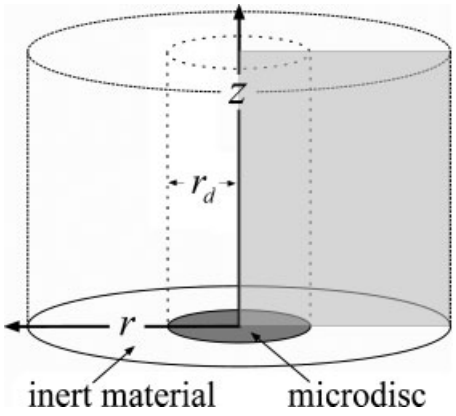

Figure 1. The coordinate system of the microdisc used in mathematical model. The plane to be simulated highlighted

The value of Γ is not permitted to go below zero and so k_b is set equal to zero once $\Gamma_{Li} = 0$ is reached. If $d\Gamma_{Li} < -k_b dt$ for any time step, dt, in the simulation, then the value k_b is adjusted so that $k_b dt = -d\Gamma_{Li} dt$.

Before the electrochemical experiment is started, we assume that the only Li present is in the form of Li^+ ions in the solution phase (bulk solution). Therefore, the initial conditions ($t = 0$) for the species taking part in the reaction are:

$$\begin{array}{llll} [Li^+] = [Li]_{bulk} & \text{for} \quad 0 \le r \le \infty & \text{and} & 0 \le z \le \infty \\ \Gamma_{Li} = 0 & \text{for} \quad 0 \le r \le r_d & \text{and} & z = 0 \end{array} \tag{6}$$

The shape of the cell implies a bulk concentration of Li^+ at the semi-infinite boundaries and non-flux boundary conditions on the symmetry axis and on the inert material surrounding the microdisc. The following equations represent these boundary conditions for $t > 0$:

$$\begin{array}{llll} [Li^+] = [Li]_{bulk} & \text{for} \quad 0 \le r \le \infty & \text{and} & z = \infty \\ [Li^+] = [Li]_{bulk} & \text{for} \quad r = \infty & \text{and} & 0 \le z \le \infty \\ \frac{\partial [Li^+]}{\partial r} = 0 & \text{for} \quad r = 0 & \text{and} & 0 \le z \le \infty \\ \frac{\partial [Li^+]}{\partial r} = 0 & \text{for} \quad r_d \le r \le \infty & \text{and} & z = 0 \end{array} \tag{7}$$

At the disc surface ($0 \le r \le r_d$, $z = 0$) we have the following condition:

$$D\frac{\partial [Li^+]}{\partial z} = \frac{\partial \Gamma_{Li}}{\partial t} = k_f [Li^+]_{z=0} - k_b \text{ for } r = 0 \text{ and } 0 \le z \le \infty \tag{8}$$

Due to these conditions the current can be calculated using the following equation:

$$I = -2\pi F \int_0^{r_d} \frac{\partial \Gamma_{Li}}{\partial t} r \, dr \tag{9}$$

Numerical simulation and convergence

A fully implicit finite difference scheme[68] combined with Newton's method and accompanied by an extended version of the Thomas algorithm[69,70] was used to solve the system of partial differential equations. The simulation space was covered with a grid that expands exponentially from the singularity (the electrode/inert material boundary) and the electrode surface.[71] The spatial and temporal convergence of the simulation program were tested to ensure a convergence error of less than 1% when compared with 'over' converged simulations. The program was written for Matlab 7.3.0 (R2006b) and executed on a PC with Pentium 4 3.40 GHz processor and 2 GB of RAM. The fitting of the simulation and experimental data were optimised by minimising the value of the mean scale difference (MSD) given by Eqn 10.

$$\text{MSD} = \sum_n \left| \frac{(I^n_{\text{experimental}} - I^n_{\text{simulation}})}{I^n_{\text{simulation}}} \right| \tag{10}$$

where n is the number of data points.

RESULTS AND DISCUSSION

CV of lithium ions in THF at Pt micro- and macro-electrodes at various temperatures

Figure 2 shows a cyclic voltammogram run at 10 mV s^{-1} using a platinum microdisc electrode (radius: 5.0 μm) in THF (0.1 M TBAP) + $LiAsF_6$ (8.14 mM) recorded between 0 and −4 V *versus* $Fc/Fc^+PF_6^-$. The temperature was maintained at 295 K ± 1 K. On the forward sweep, the current remains at baseline levels until a potential of *ca* −3.8 V *versus* $Fc/Fc^+PF_6^-$ where the reduction of Li

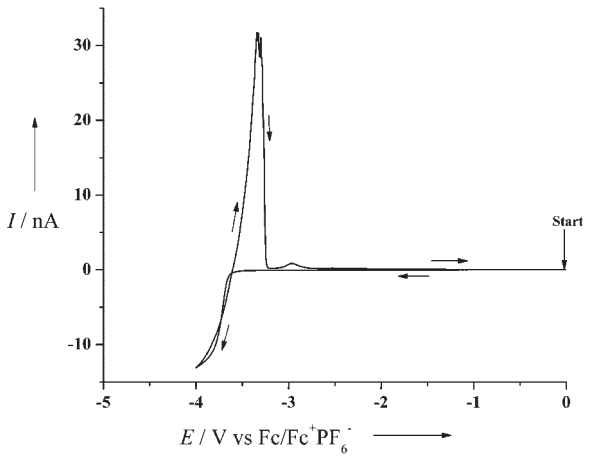

Figure 2. Reduction of lithium ions ($LiAsF_6$, 8.14 mM) in tetrahydrofuran (THF) at a platinum microdisc electrode (radius: 5.0 μm), 295 K and with tetra-*n*-butylammonium perchlorate (TBAP, 0.1 M) as the supporting electrolyte. Scan rate: 10 mV s^{-1}; start scan: 0 V, first reverse: −4 V *versus* $Fc/Fc^+PF_6^-$

DOI: 10.1002/poc

ions begins. The current value rises rapidly and continues until a current plateau is reached. In Fig. 2, it can be observed that the reduction of Li ions appears diffusion-controlled, highlighted by the current plateau at *ca* −4 V *versus* $Fc/Fc^+PF_6^-$. Determination of the diffusion coefficient, *D*, using Eqn 11, using the limiting current, I_{lim}, yielded the value, $(1 \pm 0.02) \times 10^{-5}\,cm^2\,s^{-1}$ at 295 K.

$$I_{lim} = 4nFDrc \tag{11}$$

In Eqn 11,[66] *n* is the number of electrons transferred, *F* is the Faraday's constant ($96\,485\,C\,mol^{-1}$), *c* is the concentration of electroactive species and *r* is the electrode radius. Upon reversing the electrode potential, i.e. oxidative scanning, a 'nucleation loop'[72] is first observed before the 'stripping peak'.[62] This loop is good evidence that the cathodic current is due to Li deposition; this is confirmed by the shape of the anodic (stripping) peak on the reverse scan, clearly that for the stripping of a surface layer. Table 1 provides data showing clearly that the charge involved in reduction of the Li ions is also similar in magnitude to the charge 'stripped' during oxidation or deposition. Other features of the deposition are the low background and charging currents on the forward scan and the sharp current drop following the oxidative current peak, i_p^{Ox}.

Next, a range of experiments were performed in THF at low temperatures. By varying the temperature, the influence on kinetics could be studied. The temperature was varied between 295 and 196 K. The results are shown in Figs 3 and 4. It is clear that temperature has a very strong influence on the formal potential,E_f^0, the rate of mass transport and the kinetics of the Li/Li^+ couple as observed by the current-potential curves on the reverse scans. As the temperature was decreased, the potential at which the reduction wave was observed shifted to more negative values *versus* $Fc/Fc^+PF_6^-$. Additionally, the stripping peak shifted to less negative potentials *versus* $Fc/Fc^+PF_6^-$. Figure 4 highlights the lower temperature electro-deposition data. To gain thermodynamic and kinetic data from these data, the mathematical model

Table 1. Charge (Q) injected in Coulombs for reduction/oxidation at various temperatures

Temperature/K	Charge, (Q_{red}) injected for reduction/C[a]	Charge, (Q_{ox}) injected for oxidation/C[a]
295	4.9×10^{-7}	5.1×10^{-7}
273	4.5×10^{-7}	4.4×10^{-7}
263	3.3×10^{-7}	3.5×10^{-7}
253	1.5×10^{-7}	1.6×10^{-7}
233	2.2×10^{-8}	2.0×10^{-8}
223	1.3×10^{-8}	1.6×10^{-8}
196	3.9×10^{-9}	3.8×10^{-9}

[a] Charge injected determined from analysis of the area under the peak for reduction and oxidation.

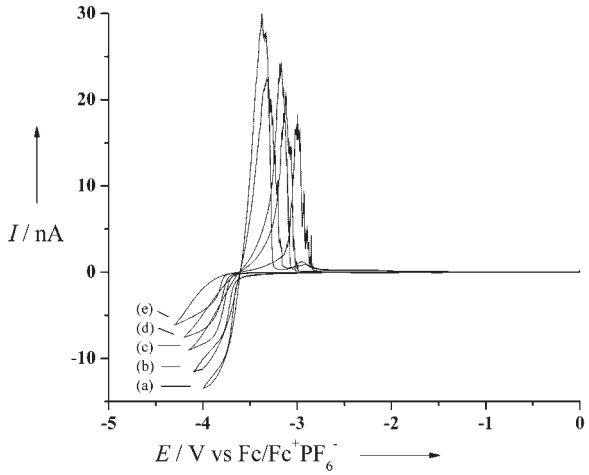

Figure 3. Reduction of lithium ions ($LiAsF_6$, 8.14 mM) in tetrahydrofuran (THF) at a platinum microdisc electrode (radius: 5.0 μm) with tetra-*n*-butylammonium perchlorate (TBAP, 0.1 M) as the supporting electrolyte. The temperature was varied: (a) 295 K, (b) 273 K, (c) 263 K, (d) 253 K and (e) 243 K. Scan rate: $10\,mV\,s^{-1}$; start scan: 0 V, first reverse: > −4 V *versus* $Fc/Fc^+PF_6^-$

described earlier in the paper was used to extract the information. The data are discussed in the next section.

A platinum macroelectrode was next used to observe the difference, if any, in the CV curves for the Li deposition. Using a larger disc electrode radius (area, $A = 0.0104\,cm^2$), the diffusion profile towards the electrode surface changes from a convergent one (microdisc electrode) to a planar regime.[65,66] The results of three scans at using different voltage scan rates are shown in Fig. 5. Immediately apparent from these curves is a 'pre-peak' before deposition peak potential, $E_p = -3.2$ V *versus* $Fc/Fc^+PF_6^-$. Determining the area under each peak (subtracting the background current and considering the

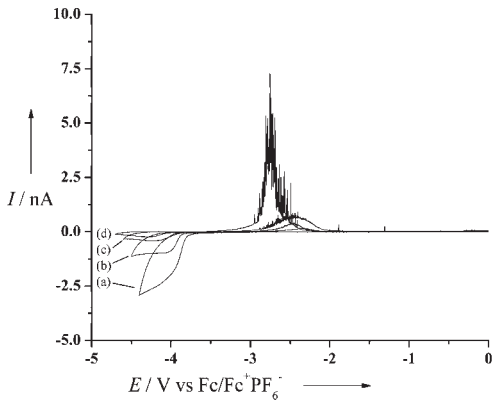

Figure 4. Reduction of lithium ions ($LiAsF_6$, 8.14 mM) in tetrahydrofuran (THF) at a platinum microdisc electrode (radius: 5.0 μm) with tetra-*n*-butylammonium perchlorate (TBAP, 0.1 M) as the supporting electrolyte. The temperature was varied: (a) 233 K, (b) 223 K, (c) 213 K and (d) 196 K. Scan rate: $10\,mV\,s^{-1}$; start scan: 0 V, first reverse: > −4 V *versus* $Fc/Fc^+PF_6^-$

DOI: 10.1002/poc

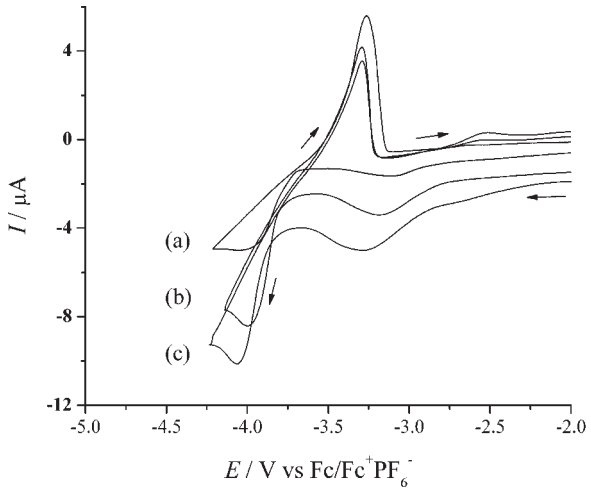

Figure 5. Reduction of lithium ions ($LiAsF_6$, 6.7 mM) in tetrahydrofuran (THF) at a platinum macrodisc electrode (area, $A = 0.0104\,cm^2$) with tetra-*n*-butylammonium perchlorate (TBAP, 0.1 M) as the supporting electrolyte at 295 K. The scan rate was varied: (a) 10; (b) 50 and (c) $100\,mV\,s^{-1}$. Start scan: -2 V, first reverse: > -4 V *versus* $Fc/Fc^+PF_6^-$

scan rate), the charge, Q, was calculated. The data are shown in Table 2.

Using the charge obtained for a scan rate of $200\,mV\,s^{-1}$, the number of moles per area was calculated to be: $7.0 \times 10^{-9}\,mol\,cm^{-2}$, and the area per mole occupied by Li is $2.6 \times 10^{-9}\,mol\,cm^2$. These data suggest that this peak is due to under-potential deposition (upd) of a Li monolayer on platinum. This also accounts for the 'post-peak' ($E_p = -3.2$ V *versus* $Fc/Fc^+PF_6^-$) observed in the microdisc electrode anodic scans where a small post-peak was seen following a larger stripping peak. The fact that bulk Li is deposited on top of upd encourages the belief in the validity of the approximation that k_f and k_b are constant for all bulk Li deposits at a given potential.

Simulation of Li deposition on platinum microdisc electrodes: variable temperature analysis for the determination of both thermodynamic (formal potential, E_f^0) and kinetic (rate constant, k_0) data

While the pre-deposition and post-stripping peaks can be attributed to the formation of a monolayer of Li on the platinum electrode the main reduction wave and stripping peak can be attributed to the deposition and stripping of bulk Li on Li. At 295 K an approximate calculation suggests that there are in the region of 2500 layers of Li on the electrode surface before the main stripping peak, although due to the radial nature of the diffusion profile to microdisc electrodes, the deposition of Li over the electrode surface will not be uniform. This confirms that the 'thick layer' model described above is appropriate. This model assumes that the deposition on the disc can be treated as having an infinitely small height and that the solution concentration of Li^+ reached near the electrode surface is well below the saturation limit. The validity of the assumptions in this model will be discussed later. Analysis of the formation of the upd monolayer of Li on the platinum microelectrode will be the subject of future investigation.

Table 2. Charge under peak in Coulombs determined at various scan rates at room temperature

Scan rate, v/mV s^{-1}	Charge, Q/C
10	2.7×10^{-5}
50	1.2×10^{-5}
100	1.8×10^{-5}
200	0.7×10^{-5}
250	0.7×10^{-5}

Figure 6 shows the formal potential, E_f^0, values (*versus* $Fc/Fc^+PF_6^-$) extracted from the experimental data shown in Fig. 2 against temperature, T. The E_f^0 values were extracted using the simulation method detailed in 'Theory' section and were optimised using a MSD method reported in 'Numerical Simulation and Convergence' section. The thermodynamic reduction potential of Li can be compared to that of various organic compounds in a common solvent system allowing a preliminary assessment of the reduction capabilities of the metal. Knowing the temperature dependence of E_f^0 allows the calculation of E_f^0 at a chosen reaction temperature. From Fig. 6 it can be seen that dE_f^0/dT equals -9.2 ($\pm$ 0.5) $\times 10^{-4}\,V\,K^{-1}$. From this the change in entropy for the half cell reaction $Li^+ + e^- = Li$ relative to the $Fc + PF_6^- = Fc^+PF_6^- + e^-$ couple can be calculated from Eqn 12 as $-89 \pm 5\,J\,mol^{-1}\,K^{-1}$.

$$\Delta S^0 = F\frac{dE_f^0}{dT} \tag{12}$$

Figure 7 shows an example of the fitting of the experimental and simulation data. Table 3 shows the best

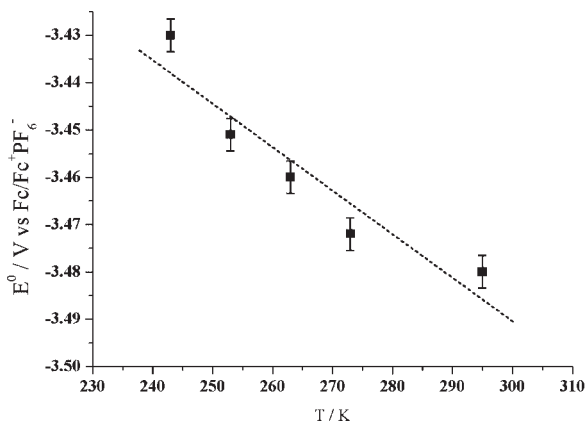

Figure 6. A plot of formal potential, E_f^0, *versus* temperature, T. From the line of best fit, $dE_f^0/dT = -9.2 \times 10^{-4}\,V\,K^{-1}$ ($R = 0.944$)

DOI: 10.1002/poc

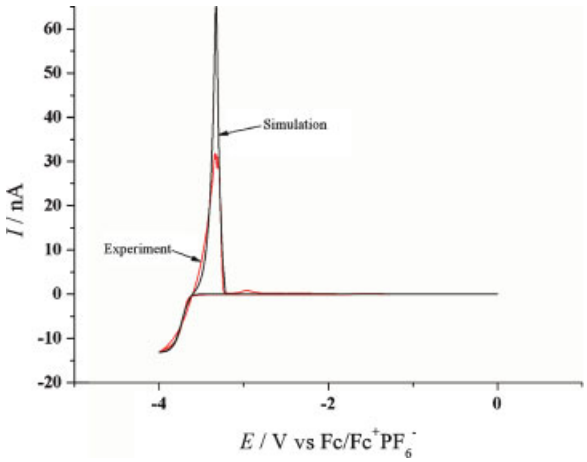

Figure 7. The fitting of simulation and experimental data at 295 K

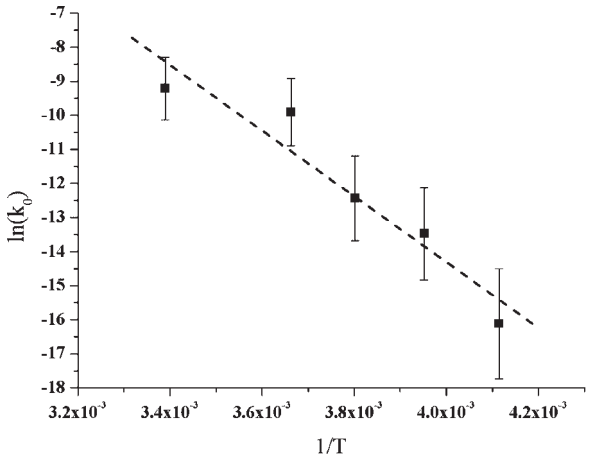

Figure 8. A plot of $\ln(k_0)$ *versus* $1/T$. From the line of best fit, $d(\ln(k_0))/d(1/T) = -9640.5$ K ($R = 0.958$)

fit values for the parameters of interest. In all cases $\alpha = 0.57 \pm 0.03$. α is the transfer coefficient, a measure of the 'symmetry' of the reaction pathway curves.[66]

Figure 8 shows the optimised k_0 values that correspond to the experimental data in Fig. 2. This is displayed as a plot of $\ln(k_0)$ against $1/T$. The linear nature of this trend corresponds to that expected from Arrhenius behaviour.

$$\ln(k) = \ln(A) - \frac{E_a}{RT} \tag{13}$$

This suggests an activation energy of $\sim 80 \pm 15\,\mathrm{kJ\,mol^{-1}}$ and a pre-exponential factor of 3.4 $(\pm 2) \times 10^{10}\,\mathrm{cm\,s^{-1}}$.

As can be seen from Fig. 7, the simulation fits the Li deposition and the early part of the stripping peak. The maximum of the latter is difficult to reproduce with the present model. This is due to a variety of reasons related to the complexity of the system under investigation and the assumptions and limitations of the model. The latter assumes that the nature of the diffusion to the microdisc is unaffected by the height of any deposits of Li on the electrode. Due to radial diffusion the current density at the edge of the microdisc is higher than that in the centre of the electrode. This results in an 'edge effect'[73] where the metal deposits in a ring around the edge of the electrode faster than it is deposited in the centre. This creates a 'wall' around the electrode which will affect the diffusion of Li^+ to the centre. The height and associated surface area of this edge deposit will also change the rate at which Li deposits and strips from around the edge of the electrode.

It is also possible that the saturation limit of Li^+ in THF may also reduce the rate at which Li can be stripped off the electrode. At 295 K the simulation calculates the concentration of Li^+ near the electrode surface to reaches 0.065 M. It is not expected that the saturation limit will have a major effect of this voltammetry in this case as Li perchlorate is known to have a high solubility in polar, aprotic solvent such as THF. Solutions up to 0.8 M $LiClO_4$ in THF have been made.[74]

In the case of Li deposition on a platinum microdisc, the process involved is more complicated than a simple heterogeneous one-electron transfer. The Li has to nucleate and deposit on the platinum electrode before Li can be deposited on itself. The nature of the film/electro deposit has been previously studied (AFM and STM analyses)[50] in a range of media and using a number of different electrode substrates.[46–49,51] These investigations have suggested that the nature of the electrode surface, i.e. surface defects,[48] the solvent/supporting electrolyte[51] and the initial electro deposits of Li, i.e. upd films will affect the resulting morphology of the

Table 3. Electochemical parameters determined from simulations at various temperatures

Temperature T/K	Diffusion coefficient, $D/\mathrm{cm^2\,s^{-1}} \pm 0.1 \times 10^{-6}$	Rate constant, $k_0/\mathrm{cm\,s^{-1}}$	Formal potential, E^0_f/V *versus* $Fc/Fc^+PF_6^-$
295	8.7×10^{-6}	1.0×10^{-4}	−3.480
273	7.6×10^{-6}	5.0×10^{-5}	−3.472
263	6.0×10^{-6}	4.0×10^{-6}	−3.460
253	5.0×10^{-6}	1.4×10^{-6}	−3.451
243	4.0×10^{-6}	1.0×10^{-7}	−3.430

DOI: 10.1002/poc

multilayer structure. In the stripping peak there will be a mixture of Li stripping off Li and off the platinum electrode. Therefore, the use of a simple rate constant, to cover this type of behaviour is clearly approximate.

At low temperatures (below 233 K) the model is not valid as only very small amounts of Li are deposited on the electrode and the voltammetry is dominated because the nucleation processes.

CONCLUSIONS

The kinetic and thermodynamic data presented in this paper provide a basis for the understanding of the use of the Li/Li$^+$ couple in synthetic chemistry and electrochemistry.

Acknowledgements

CAP and FLB thank EPSRC for joint project studentships (GR/T05011/01). SEWJ thanks the NERC for a studentship (NER/S/A/2005/13354).

REFERENCES

1. Tomooka K, Ito M. *Main Group Met. Chem.* 2004; **1**: 1.
2. Yus M, Foubelo F. *Targets Heterocycl. Syst.* 2002; **6**: 136.
3. Nudelman NS, Velurtas S, Grela MA. *J. Phys. Org. Chem.* 2003; **16**: 669.
4. Maercker A, Reider K, Girreser U. In *Organosilicon Chemistry III: From Molecules to Materials*, Conference, Auner N, Weis J (eds). Siegen: Germany, 1996; 195.
5. Zhao H, Li D-J, Deng L, Liu L, Guo Q-X. *Chem. Commun.* 2003; **4**: 506.
6. Ranu BC, Dutta J, Jana U. *J. Indian Inst. Sci.* 2001; **81**: 139.
7. Kawase T, Kurata H, Fujino S, Ekinaka T, Oda M. *Tetrahedron Lett.* 1992; **33**: 7201.
8. Burke SD, Danheiser RL. *Oxidizing and Reducing Agents: Handbook of Reagents for Organic Synthesis*. Wiley: New York, 1999.
9. Guijarro A, Yus M. *Tetrahedron Lett.* 1994; **50**: 3447.
10. Wu G, Huang M. *Chem. Rev.* 2006; **106**: 2596.
11. Yang A, Butela H, Deng K, Doubleday MD, Cohen T. *Tetrahedron* 2006; **62**: 6526.
12. Yus M, Herrera RP, Guijarro A. *Chem. Eur. J.* 2002; **8**: 2574.
13. Yus M, Martinez P, Guijarro A. *Syn. Commun.* 2003; **33**: 2365.
14. Yus M, Moreno B, Foubelo F. *Synthesis* 2004; **7**: 1115.
15. Freeman PK, Hutchinson LL. *Tetrahedron Lett.* 1976; **22**: 1849.
16. Freeman PK, Hutchinson LL. *J. Org. Chem.* 1980; **45**: 1924.
17. Andrieux CP, Robert M, Savéant J-M. *J. Am. Chem. Soc.* 1995; **117**: 9340.
18. Macias-Ruvalcaba NA, Evans DH. *J. Phys. Chem. B* 2005; **109**: 14642.
19. Casado F, Pisano L, Farriol M, Gallardo I, Marquet J, Melloni G. *J. Org. Chem.* 2000; **65**: 322.
20. Nagaoka T, Okasaki S. *J. Electroanal. Chem.* 1983; **158**: 139.
21. Khoo SB, Foley JK, Pons S. *J. Electroanal. Chem.* 1986; **215**: 273.
22. Oyama M, Webster RD, Suárez M, Marken F, Compton RG. *J. Phys. Chem. B* 1998; **102**: 6588.
23. Kerdpaiboon N, Tomapatanaget B, Chailapakul O, Tuntulani T. *J. Org. Chem.* 2005; **70**: 4797.
24. Wain AJ, Wildgoose GG, Heald CGR, Jiang L, Jones TGJ, Compton RG. *J. Phys. Chem. B* 2005; **109**: 3971.
25. Richards JA, Evans DH. *J. Electroanal. Chem.* 1977; **81**: 171.
26. Goulart MOF, Utley JHP. *J. Org. Chem.* 1988; **53**: 2520.
27. Neudörffer A, Deguin B, Hamel C, Fleury M-B, Largeron M. *Collect. Czech. Chem. Commun.* 2003; **68**: 1515.
28. Neudörffer A, Fleury M-B, Desvergne J-P, Largeron M. *Electrochim. Acta* 2006; **52**: 715.
29. Schafer U. In *Mengen- und Spurenelemente, Arbeitstagung, 16th, Jena*, Manfred A (ed.). Leipzig: Germany, 1996; 752.
30. Wang Q, Sun J, Chen C. *J. Power Sources* 2006; **162**: 1363.
31. Morford RV, Welna DT, Kellam CE, III., Hofmann MA, Allock HR. *Solid State Ionics* 2006; **177**: 721.
32. Wang QS, Sun JH, Yao XL, Chen CH. *Thermochim. Acta 437* 2005; **1–2**: 12.
33. Aurbach D, Gofer Y, Lu Z, Schechter A, Chusid O, Gizbar H, Cohen Y, Ashkenazi V, Moshkovich M, Turgeman R, Levi E. *J. Power Sources* 2001; **97–98**: 28.
34. Jansen AN, Kahaian AJ, Kepler KD, Nelson PA, Amine K, Dees DW, Vissers DR, Thackeray MM. *J. Power Sources* 1999; **81–82**: 902.
35. Pistola G, Nazri G-A. *Lithium Batteries: Science and Technology.* Springer: New York, 2004.
36. Abraham KM, Foos JS, Goldman JR. *J. Electrochem. Soc.* 1984; **131**: 2197.
37. Abraham KM, Harris PB, Natwig DL. *J. Electrochem. Soc.* 1983; **130**: 2309.
38. Goldman JR, Mank RM, Young JH, Koch VR. *J. Electrochem. Soc.* 1980; **127**: 1461.
39. Koch VR, Goldman JR, Mattos CJ, Mulvaney M. *J. Electrochem. Soc.* 1982; **129**: 1.
40. Abraham KM, Goldman JR, Natwig DL. *J. Electrochem. Soc.* 1982; **129**: 2404.
41. Abraham KM, Goldman JR, Dempsey MD. *J. Electrochem. Soc.* 1981; **128**: 2493.
42. Koch VR, Young JH. *Science* 1979; **204**: 499.
43. Koch VR. *J. Electrochem. Soc.* 1979; **125**: 181.
44. Koch VR, Young JH. *J. Electrochem. Soc.* 1978; **125**: 1371.
45. Koch VR, Brummer SB. *Electrochimic. Acta* 1978; **23**: 55.
46. Muhammad J. *J. Pure Appl. Sci.* 2003; **22**: 75.
47. Saito T, Uosaki K. *J. Electrochem. Soc.* 2003; **150**: A532.
48. Farias D, Braun K-F, Folsch S, Meyer G, Reider K-H. *Surface Sci.* 2000; **470**: L93.
49. Ribes AT, Beaunier P, Willmann P, Lemordant D. *J. Power Sources* 1996; **58**: 189.
50. Morigaki K, Kabuto N, Yoshino K, Ohta A. *Power Sources* 1995; **15**: 267.
51. Aubay M, Lojou E, Messina R, Perichon J. *J. Electrochem. Soc.* 1993; **140**: 879.
52. Takei T. *J. Appl. Electrochem.* 1979; **9**: 587.
53. Paddon CA, Silvester DS, Bhatti FL, Donohoe TJ, R. Compton G. *Electroanalysis* 2007; **19**: 11.
54. Fietkau N, Paddon CA, Bhatti FL, Donohoe TJ, Compton RG. *J. Electroanal. Chem.* 2006; (in press).
55. Paddon CA, Bhatti FL, Donohoe TJ, Compton RG. *J. Electroanal. Chem.* 2006; **589**: 187.
56. Paddon CA, Bhatti FL, Donohoe TJ, Compton RG. *Chem. Comm.* 2006; **32**: 3402.
57. Baranski AS, Drogowska MA, Fawcett WR. *J. Electroanal. Chem.* 1986; **215**: 237.
58. Wiesener K, Eckoldt U, Rahner D. *Electrochimic. Acta* 1989; **34**: 1277.
59. Aojula KS, Pletcher D. *J. Chem. Soc. Faraday Trans.* 1990; **86**: 1851.
60. Aojula KS, Genders DJ, Holding AD, Pletcher D. *Electrochimic. Acta* 1989; **34**: 1535.
61. Hedges WM, Pletcher D. *J. Chem. Soc. Faraday Trans.* 1986; **82**: 179.
62. Genders DJ, Hedges WM, Pletcher D. *J. Chem. Soc. Faraday Trans.* 1984; **80**: 3399.
63. Pangborn AB, Giardello MA, Grubbs RK, Rosen RK, Timmers RJ. *Organometallics* 1996; **15**: 1518.
64. Paddon CA, Compton RG. *Electroanalysis* 2005; **21**: 1919.
65. Bard AJ, Stratmann M, Schafer JH. *Encyclopedia of Electrochemistry, Volume 8, Organic Electrochemistry.* Wiley: New York, 2004.
66. Bard AJ, Faulkner LR. *Electrochemical Methods: Fundamentals and Applications*, 2nd edn. John Wiley & Sons: New York, 2001.

DOI: 10.1002/poc

67. Davies TJ, Brookes BA, Fisher AC, Yunus K, Wilkins SJ, Greene PR, Wadhawan JD, Compton RG. *J. Phys. Chem. B* 2003; **107**: 6431.
68. Strikwerda. *Finite Difference Schemes and Partial Differential Equations*. Wadsworth & Brookes/Cole: London, 1989.
69. Kreiszig E. *Advanced Engineering Mathematics*. John Wiley and Sons: New York, 1962.
70. Svir IB, Klymenko OV, Compton RG. *Radiotekhnika* 2001; **118**: 92.
71. Gavaghan DJ. *J. Electroanal. Chem.* 1998; **456**: 1.
72. Heinze J, Rasche A, Pagels M, Geschke B. *J. Phys. Chem. B* 2007; **111**: 989–999.
73. Simm AO, Banks CE, Ward-Jones S, Davies TJ, Lawrence NS, Jones TGJ, Jiang L, Compton RG. *Analyst (Cambridge, United Kingdom)* 2005; **130**: 1303.
74. Bennouna M, Beuzelin P, Cachet H, Lestrade JC, Gastaud C, Redon M. *Int. J. Infrar. Millim. Wave.* 1980; **1**: 319.

DOI: 10.1002/poc